

Article

Maximizing Efficient Power for an Irreversible Porous Medium Cycle with Nonlinear Variation of Working Fluid's Specific Heat

Pengchao Zang^{1,2,3}, Lingen Chen^{1,2,3,*} and Yanlin Ge^{1,2,3}¹ Institute of Thermal Science and Power Engineering, Wuhan Institute of Technology, Wuhan 430205, China² Hubei Provincial Engineering Technology Research Center of Green Chemical Equipment, Wuhan 430205, China³ School of Mechanical & Electrical Engineering, Wuhan Institute of Technology, Wuhan 430205, China

* Correspondence: lingenchen@hotmail.com

Abstract: Considering the specific heat characteristics of working fluid and existence of various losses in a porous medium (PM) cycle, this paper applies finite time thermodynamic theory to study its efficient power performance with nonlinear variable specific heat model. Range of the cycle pre-expansion ratio is obtained by solving the equation, and PM cycle is converted to Otto cycle by choosing appropriate pre-expansion ratio. Influences of pre-expansion ratio, specific heat characteristics, temperature ratio, and various losses on cycle performances are investigated. Thermal efficiencies are compared at operating points of the maximum power output and efficient power. The results show that PM cycle has better performance than Otto cycle. Under certain conditions of parameters, thermal efficiencies at the maximum efficient power and maximum power output operating points are 50.45% and 47.05%, respectively, and the former is 7.22% higher than the latter. The engine designed with the maximum efficient power as the criterion can improve thermal efficiency by losing less power output. The results of this paper can guide parameters selection of actual PM heat engine.



Citation: Zang, P.; Chen, L.; Ge, Y. Maximizing Efficient Power for an Irreversible Porous Medium Cycle with Nonlinear Variation of Working Fluid's Specific Heat. *Energies* **2022**, *15*, 6946. <https://doi.org/10.3390/en15196946>

Academic Editors: Urmila Diwekar and Debangsu Bhattacharyya

Received: 24 August 2022

Accepted: 21 September 2022

Published: 22 September 2022

Publisher's Note: MDPI stays neutral with regard to jurisdictional claims in published maps and institutional affiliations.



Copyright: © 2022 by the authors. Licensee MDPI, Basel, Switzerland. This article is an open access article distributed under the terms and conditions of the Creative Commons Attribution (CC BY) license (<https://creativecommons.org/licenses/by/4.0/>).

Keywords: porous medium cycle; finite time thermodynamics; efficient power; nonlinear variable specific heat; optimal performance; performance comparison

1. Introduction

Finite time thermodynamics (FTT) [1–11] has attained significant progress in recent years. Many scholars have applied FTT to research performances of thermodynamic cycles, including optimal performance studies [12–29] and optimal path studies [30–42]. Early research work on the internal combustion engine cycles mainly focused on thermal efficiency (η) and power output (P) under the condition of constant specific heat (SH) of working fluid (WF) [43]. When actual heat engines are working, the change in SH of WF is very complicated. In order to study the effects of the SH of WF changing with temperature, which is closer to engineering practice, some scholars have put forward linear [44] and nonlinear [45] models of SH of WFs varying with temperature. In addition to considering the effects of the WF's SH characteristics on the performances of thermodynamic cycles, it is crucial to take into account the influences of different losses and different objective functions (OFs) on the cycle performance. Common loss models include heat transfer loss (HTL) [43], internal irreversibility loss (IIL) [46], and friction loss (FL) [47]. Common OFs include P and η [48], ecological function (E) [49], power density (P_d) [50], efficient power (E_p) [51], etc.

Many scholars have studied the P , η , P_d , and E_p optimal performances of the internal combustion engine cycles by applying FTT theory. With the P_d as the OO, Gonca and Genc [52,53] studied the optimal performances of the Gas-Mercury-Steam system and the double-reheat Rankine cycle. Chen et al. [54] derived the P , η , E , and P_d of an irreversible modified closed Brayton cycle. Diskin and Tartakovsky [55] introduced the low dissipation

model and electrochemistry into the performance optimization of the otto cycle and investigated the η at the maximum P operating point. Wang et al. [56] established irreversible Lenoir cycle with changing temperature heat reservoirs and investigated its P and η . Gonca et al. [57] combined the Dual cycle and the Diesel cycle and derived the P , exergy efficiency, and P_d of a Dual-Diesel cycle. Sahin [58] analyzed the effects of parameters such as compression ratio equivalence ratio cylinder temperature on the P , P_d , and effective ecological P_d of a modified Dual cycle. Paul et al. [59] investigated the P of Stirling cycle by applying optimal control theory. Bellos et al. [60] analyzed and optimized the η of a solar-fed organic Rankine cycle, and compared it with the η of organic Rankine cycle

Yan et al. [51] first took the product of cycle P and η as OF and introduced this OF into the study of an endoreversible Carnot heat engine. Yilmaz [61] named this OF as E_p for the first time. Atmaca et al. [62] studied the P_d and the E_p of a reversible dual cycle without any loss. Reyes-Ramírez et al. [63] studied the P , E_p , and E of a Curzon-Ahlborn heat engine. Kumar et al. [64] derived the E_p and the P_d of an endoreversible Brayton. Gonca [65] analyzed effects of piston speed, pressure ratio, and intake temperature on E_p of an irreversible Atkinson cycle. Gonca and Hocaoglu [66] combined the Miller cycle and the Diesel cycle and derived the E_p , E_p density, and effective η of a Diesel-Miller cycle. Gonca and Sahin [67,68] investigated the P , η E_p , effective P_d , and exergy efficiency of Miller-Takemura cycle. Nilavarasi and Ponmurugan [69] introduced E_p into the optimization of a dissipative Carnot cycle.

Ferrenberg [70] put forward the porous medium (PM) engine. Based on PM combustion technology [71], this engine had the characteristics of high efficiency, low emissions, low noise, and stable combustion. Durst et al. [72] simulated how the PM engine operated by modifying the Diesel engine and demonstrated performance of PM engine. Liu et al. [73] studied P and η performances of reversible PM engine.

Based on the FTT theory, Liu et al. [74] and Ge et al. [75] studied P and η of endoreversible [74] and irreversible [75] PM cycles. When the WF's SH is constant with temperature, Zang et al. [76] analyzed effects of irreversibility losses, temperature ratio, and pre-expansion ratio on P_d , and conducted multi-objective optimization on P , η , P_d , and E for irreversible PM cycle. Considering WF's SH is linear variable with its temperature, Zang et al. [77] derived E and P_d , compared P and η in the circumstances of maximum η , maximum P , maximum E and maximum P_d , and performed multi-objective optimization on P , η , P_d , and E for irreversible PM cycle.

In the aforementioned literature, there is no report on the E_p performance optimization for irreversible PM engine. Based on [75–77], this paper will analyze the cycle maximum E_p performance when WF's SH is nonlinear variable with its temperature [45] and compare η at the maximum E_p ($(E_p)_{\max}$) working point and the maximum P (P_{\max}) working point.

2. Model of PM

Irreversible PM cycle model shown in Figure 1 contains two constant volume processes 2 – 3 and 5 – 1; isothermal endothermic process 3 – 4; irreversible adiabatic compression process 1 – 2; and adiabatic expansion process 4 – 5. It can be seen from Figure 1 that $v_1 = v_5$, $v_2 = v_3$, $T_3 = T_4$, $p_1 = p_5$, and $p_2 = p_3$, where v is specific volume, T is temperature, and p is pressure.

The cycle pre-expansion ratio (ρ), temperature ratio (τ), and compression ratio (γ) are expressed as:

$$\rho = V_4/V_3 \quad (1)$$

$$\tau = T_3/T_1 \quad (2)$$

$$\gamma = V_1/V_2 \quad (3)$$

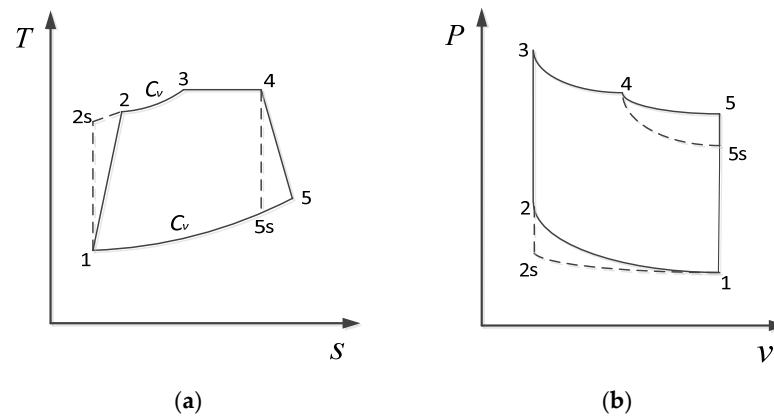


Figure 1. $p - v$ and $T - s$ diagrams. (a) $T - s$ diagram. (b) $P - v$ diagram.

Constant volume SH and constant pressure SH have a following relationship:

$$C_v = C_p - R \tag{5}$$

In earlier studies [62–64], it was assumed that the WF’s SH was constant when the temperature range was small, but this assumption does not hold for large temperature changes in actual cycles. According to [45], assuming that the SH of the WF is only related to the temperature and has a nonlinear relationship with temperature, the constant pressure SH of the WF can be expressed as:

$$C_p = a_1 T^2 + a_2 T^{1.5} + a_3 T + a_4 T^{0.5} + a_5 + a_6 T^{-1.5} + a_7 T^{-2} + a_8 T^{-3} \tag{4}$$

where $a_1 - a_8$ are constants.

where R is gas constant.

According to Equations (4) and (5), the constant volume SH can be expressed as:

$$C_v = a_1 T^2 + a_2 T^{1.5} + a_3 T + a_4 T^{0.5} + a_5 - R + a_6 T^{-1.5} + a_7 T^{-2} + a_8 T^{-3} \tag{6}$$

The heat absorption rate is:

$$Q_{in} = \dot{m} \left(\int_{T_2}^{T_3} C_v dT + MRT_3 \ln \rho \right) = \dot{m} \int_{T_2}^{T_3} (7.2674 \times 10^{-10} T^2 + 4.2166 \times 10^{-6} T^{1.5} - 1.23134 \times 10^{-5} T + 9.1698 \times 10^{-4} T^{0.5} + 30.2642 - 4.3848 \times 10^5 T^{-1.5} + 8.8827 \times 10^6 T^{-2} - 6.4148 \times 10^8 T^{-3}) dT \tag{7}$$

$$= \dot{m} [2.422 \times 10^{-10} T^3 + 1.6866 \times 10^{-6} T^{2.5} - 6.1567 \times 10^{-6} T^2 + 6.1132 \times 10^{-4} T^{1.5} + 30.2642 T + 8.7696 \times 10^5 T^{-0.5} - 8.8827 \times 10^6 T^{-1} + 3.2074 \times 10^8 T^{-2}]_{T_2}^{T_3} + MRT_3 \ln \rho$$

The heat release rate is:

$$Q_{out} = \dot{m} \int_{T_1}^{T_5} C_v dT = \dot{m} \int_{T_1}^{T_5} (7.2674 \times 10^{-10} T^2 + 4.2166 \times 10^{-6} T^{1.5} - 1.23134 \times 10^{-5} T + 9.1698 \times 10^{-4} T^{0.5} + 30.2642 - 4.3848 \times 10^5 T^{-1.5} + 8.8827 \times 10^6 T^{-2} - 6.4148 \times 10^8 T^{-3}) dT \tag{8}$$

$$= \dot{m} [2.422 \times 10^{-10} T^3 + 1.6866 \times 10^{-6} T^{2.5} - 6.1567 \times 10^{-6} T^2 + 6.1132 \times 10^{-4} T^{1.5} + 30.2642 T + 8.7696 \times 10^5 T^{-0.5} - 8.8827 \times 10^6 T^{-1} + 3.2074 \times 10^8 T^{-2}]_{T_1}^{T_5}$$

where \dot{m} is the mass flow rate.

Compression and expansion efficiencies are used to represent IIL of PM cycle for the processes 1 – 2 and 4 – 5.

$$\eta_c = (T_{2s} - T_1) / (T_2 - T_1) \tag{9}$$

$$\eta_e = (T_5 - T_4) / (T_{5s} - T_4) \tag{10}$$

where η_c is compression efficiency and η_e is expansion efficiency.

According to [44], it is presumed that the variable SH process of the WF is composed of an infinite number of infinitely small constant SH processes of the WF, and one has:

$$TV^{k-1} = (T + dT)(V + dV)^{k-1} \quad (11)$$

$$C_v \ln T_j/T_i = R \ln V_i/V_j \quad (12)$$

where $T = (T_i - T_j)/\ln(T_i/T_j)$ is the temperature logarithmically on average between states i and j .

According to Equations (7) and (8) and the processes $1 \rightarrow 2s$ and $4 \rightarrow 5s$, one has:

$$C_v \ln(T_{2s}/T_1) = R \ln \gamma \quad (13)$$

$$C_v \ln(T_4/T_{5s}) = R \ln(\gamma/\rho) \quad (14)$$

According to [43], the HTL between the WF and ambient through the cylinder cannot be ignored, and one has:

$$\dot{Q}_{leak} = (B/2)(T_2 + T_3 - 2T_0) = (T_2 + T_3 - 2T_0)B_1 \quad (15)$$

where T_0 is ambient temperature and B is HTL coefficient.

According to [46], the FL due to the movement of the cylinder wall and piston cannot be ignored, and one has:

$$P_\mu = 4\mu(4Ln)^2 = 64\mu(Ln)^2 \quad (16)$$

where n is rotation speed and L is stroke length.

The P , η , and E_p expressions are shown in Appendix A.

It can be seen from Figure 1 that state point 3 is located between state points 4 and 2, so the value range of ρ is:

$$1 \leq \rho \leq V_4/V_2 \quad (17)$$

The P and E_p after dimensionless processing can be expressed as:

$$\bar{P} = P/P_{\max} \quad (18)$$

$$\bar{E}_p = E_p/(E_p)_{\max} \quad (19)$$

3. Efficient Power Maximization

According to [45,63,65], the parameters are as follows: $a_1 = 7.2674 \times 10^{-10}$, $a_2 = 4.2166 \times 10^{-6}$, $a_3 = -1.23134 \times 10^{-5}$, $a_4 = 9.1698 \times 10^{-4}$, $a_5 = 38.5787$, $a_6 = -4.3848 \times 10^5$, $a_7 = 8.8827 \times 10^6$, $a_8 = -6.4148 \times 10^8$, $T_0 = 300$ K, $T_1 = 350$ K, $\rho = 1 - 1.6$, $\tau = 5.78 - 6.78$, $B = 2.2$ W/K, $\mu = 1.2$ kg/s, $n = 30$ s⁻¹, $L = 0.07$ m, and $\dot{m} = 1$ mol/s.

Figure 2 shows the influence of cycle τ on the \bar{E}_p characteristics. The figure shows that the curve of the relationship between the \bar{E}_p and γ ($\bar{E}_p - \gamma$) is a parabolic-like one, and it exists an optimal γ ($\gamma_{\bar{E}_p}$) which can make the \bar{E}_p reach the maximum ($(\bar{E}_p)_{\max}$). The curve of the relationship between the \bar{E}_p and η ($\bar{E}_p - \eta$) is a loop-shaped one which has the maximum η (η_{\max}) working point and the $(\bar{E}_p)_{\max}$ working point. The corresponding η at the $(\bar{E}_p)_{\max}$ working point is $(\eta_{\bar{E}_p})$, and the corresponding η at the \bar{P}_{\max} working point is $\eta_{\bar{P}}$. As τ increases, both $\gamma_{\bar{E}_p}$ and $\eta_{\bar{E}_p}$ increase. As τ increases from 5.78 to 6.78, $\gamma_{\bar{E}_p}$ increases from 17.2 to 23.8, and $\eta_{\bar{E}_p}$ increases from 0.4851 to 0.5213, by an increase of about 8.20%.

Figure 3 shows influences of cycle ρ on \bar{E}_p characteristics. $\rho = 1$ is performance curve of Otto engine cycle. As ρ increases, both $\gamma_{\bar{E}_p}$ and $\eta_{\bar{E}_p}$ increase. As ρ increases from 1.2 to 1.6, $\gamma_{\bar{E}_p}$ increases from 20.4 to 24.4, and $\eta_{\bar{E}_p}$ increases from 0.5045 to 0.5285, by an increase of about 4.76%.

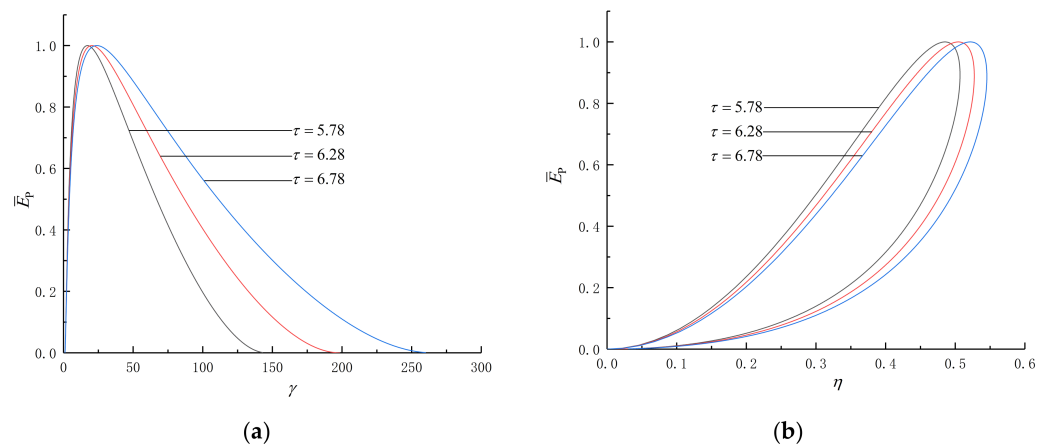


Figure 2. Effects of τ on $\bar{E}_p - \gamma$ and $\bar{E}_p - \eta$. (a) Variation of \bar{E}_p with γ . (b) Variation of \bar{E}_p with η .

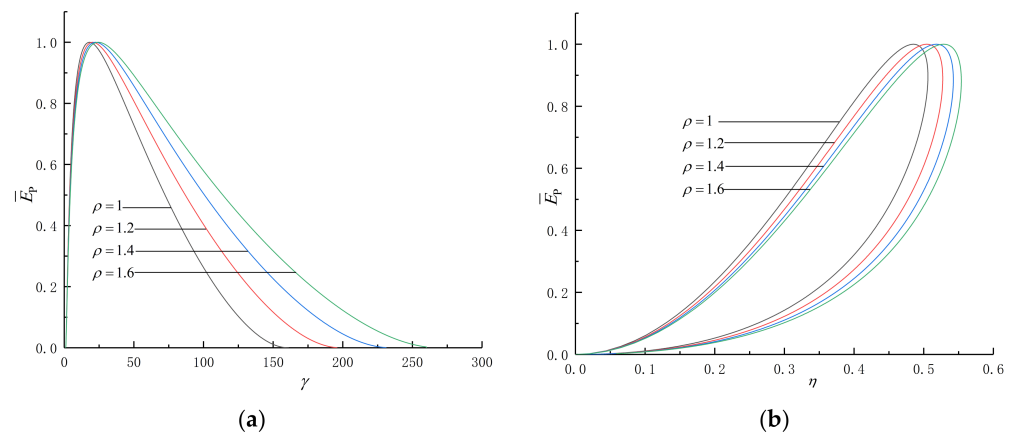


Figure 3. Effects of ρ on $\bar{E}_p - \gamma$ and $\bar{E}_p - \eta$. (a) Variation of \bar{E}_p with γ . (b) Variation of \bar{E}_p with η .

Figure 4 shows the influences of different losses on the $\bar{E}_p - \gamma$ and $\bar{E}_p - \eta$. Table 1 lists the $\gamma_{\bar{E}_p}$ and $\eta_{\bar{E}_p}$ obtained when different losses are considered. It can be seen from Table 1 that with the increase of loss items considered, both $\gamma_{\bar{E}_p}$ and $\eta_{\bar{E}_p}$ decrease, among which η_c , η_e , and B have bigger effect on $\gamma_{\bar{E}_p}$ and $\eta_{\bar{E}_p}$, and μ has a small effect on $\gamma_{\bar{E}_p}$ and $\eta_{\bar{E}_p}$. When the three losses are considered at the same time, the $\gamma_{\bar{E}_p}$ is reduced by 32.56% and the $\eta_{\bar{E}_p}$ is reduced by 25.41%.

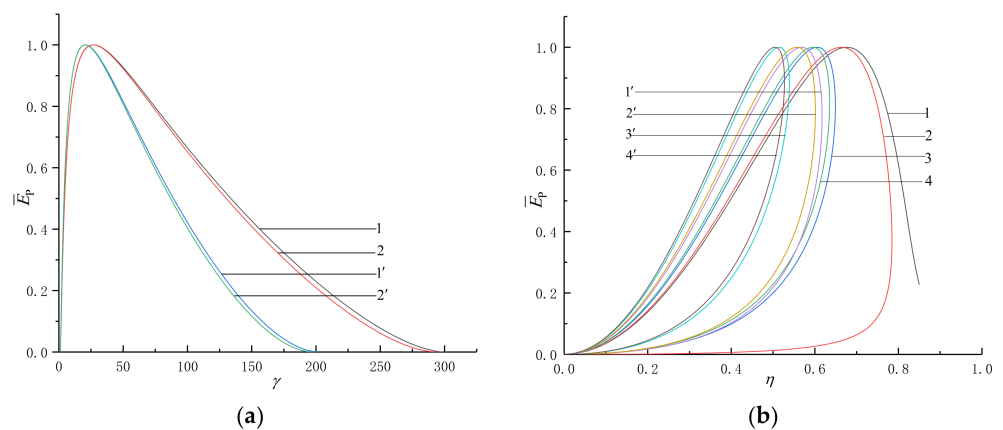


Figure 4. Effects of η_c , η_e , B and μ on $\bar{E}_p - \gamma$ and $\bar{E}_p - \eta$. (a) $\bar{E}_p - \gamma$. (b) $\bar{E}_p - \eta$.

Table 1. Comparison of the $\gamma_{\bar{E}_P}$ and $\eta_{\bar{E}_P}$ when considering different losses.

Curve	Losses Considered	$\gamma_{\bar{E}_P}^-$	Percentage of $\gamma_{\bar{E}_P}$ Reduction	$\eta_{\bar{E}_P}^-$	Percentage of $\eta_{\bar{E}_P}$ Reduction
1	Without any losses	30.1	0.00%	67.61%	0.00%
2	Friction	29.6	1.66%	66.32%	1.91%
3	Heat transfer	27.0	10.30%	60.56%	10.29%
4	Friction and heat transfer	26.7	11.30%	59.49%	12.01%
1'	Internal irreversibility	22.3	25.91%	56.85%	15.91%
2'	Internal irreversibility and friction	22.0	26.91%	55.68%	17.65%
3'	Internal irreversibility and heat transfer	20.6	31.56%	51.46%	23.89%
4'	Friction, heat transfer, and internal irreversibility	20.3	32.56%	50.42%	25.41%

Figure 5 shows the influences of τ and ρ on η_p and η_{E_p} . As can be seen from the Figure 5a,b, no matter how τ and ρ change, η_{E_p} is always greater than η_p .

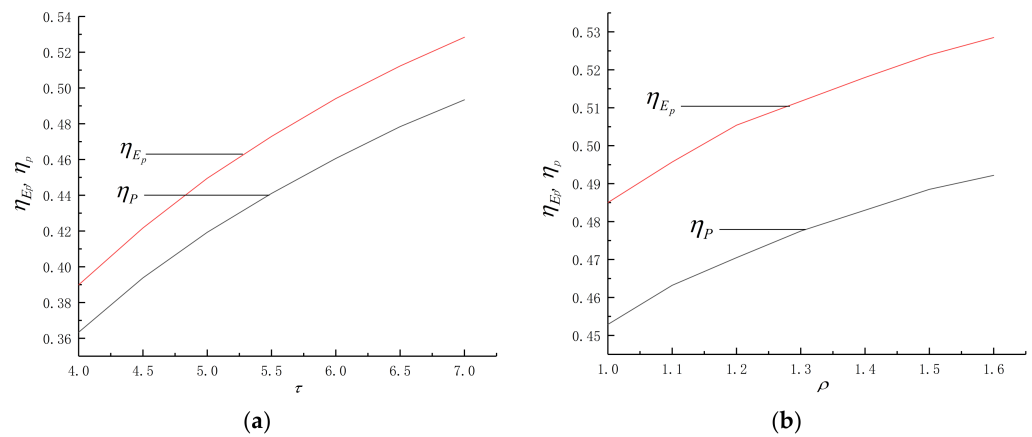


Figure 5. Effects of τ and ρ on η_{E_p} and η_p . (a) Effect of τ . (b) Effect of ρ .

Figure 6 shows the relationships between $\bar{P} - \eta$ and $\bar{E}_P - \eta$ when the cycle design parameters are constants. The results show that $\eta_{\bar{P}}$ is 47.05%, and $\eta_{\bar{E}_P}$ is 50.45%. The latter is about 7.22% higher than the former. The \bar{P} is 0.9739 under the condition of $(\bar{E}_P)_{max}$, by a decrease of 2.61%. Compared with the P_{max} condition, the PM cycle sacrifices part of the power output under the $(\bar{E}_P)_{max}$ condition, but the cycle η can be greatly improved. The E_P objective function reflects compromise between η and P .

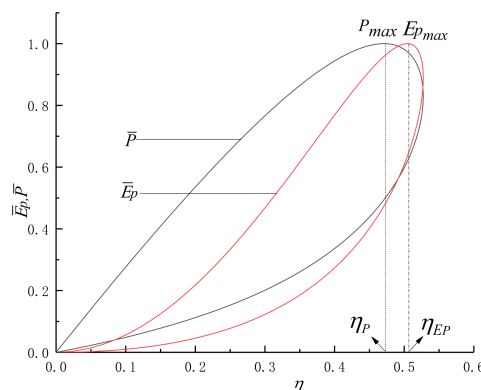


Figure 6. The relationships of $\bar{P} - \eta$ and $\bar{E}_P - \eta$.

4. The Influences of SH Characteristics on Cycle Performance

Figure 7 shows the comparisons of P and η of irreversible PM cycle with constant SH ($P_{\text{const}}, \eta_{\text{const}}$), with linear variable SH ($P_{\text{linear}}, \eta_{\text{linear}}$), and with nonlinear variable SH ($P_{\text{nonlinear}}, \eta_{\text{nonlinear}}$). The performance indicators for the former two cases are shown in and Appendix B.

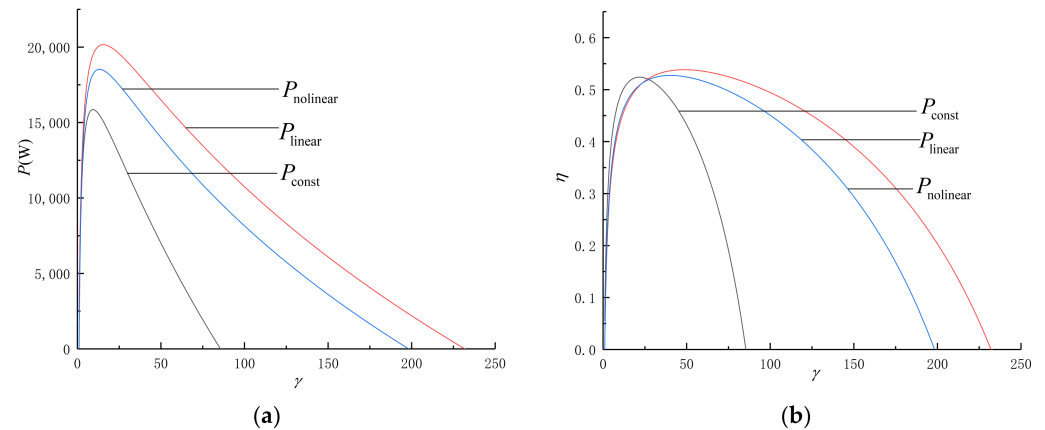


Figure 7. Effects of variable SH of WF on P and η . (a) Effects of variable SH of WF on P . (b) Effects of variable SH of WF on η .

Table 2 lists the maximum P and maximum η under the three kinds of SH models are obtained by deriving the γ . $P_{\text{linear, max}}$ is 27.14% larger than $P_{\text{const, max}}$, $P_{\text{nonlinear, max}}$ is 16.83% larger than $P_{\text{const, max}}$, and $P_{\text{linear, max}}$ is 8.82% larger than $P_{\text{nonlinear, max}}$. $\eta_{\text{linear, max}}$ is 2.73% larger than $\eta_{\text{const, max}}$, $\eta_{\text{nonlinear, max}}$ is 0.63% larger than $\eta_{\text{const, max}}$, and $\eta_{\text{linear, max}}$ is 2.09% larger than $\eta_{\text{nonlinear, max}}$.

Table 2. Maximum values of P and η of the three cycle models.

Maximum Power Output	Maximum Value	Maximum Efficiency	Maximum Value
$P_{\text{const, max}}$	15,858 W	$\eta_{\text{const, max}}$	0.5240
$P_{\text{linear, max}}$	20,162 W	$\eta_{\text{linear, max}}$	0.5383
$P_{\text{nonlinear, max}}$	18,527 W	$\eta_{\text{nonlinear, max}}$	0.5273

It is assumed that the WF's SH is constant when the temperature range is small, but this assumption does not hold for large temperature changes in actual cycles. It can be seen from Figure 7 and Table 2 that the influences of different models of SH on cycle performance is very obvious. The model with nonlinear variation of WF's SH is more suitable for the working state of the actual heat engine.

5. Conclusions

Applying FTT, the E_p objective function is introduced into the study of optimal performances of an irreversible PM engine cycle, and E_p expression is derived. The effects of τ , ρ , three kind of losses, and WF's variable SH characteristics on E_p versus γ and η are analyzed, and the performance difference of the cycle under the condition of P_{max} and $(E_p)_{\text{max}}$ are compared. The nonlinear variable SH model of WF with its temperature is adopted for irreversible PM cycle, which is closer to the actual working state of heat engines. The results show that:

1. The $\bar{P}_d - \eta$ and $\bar{P}_d - \gamma$ curves of the cycle are a loop-shaped one and parabolic-like one, respectively. As ρ and τ increase, both $\gamma_{\bar{E}_p}$ and $\eta_{\bar{E}_p}$ increase. As b_v and k_1 decrease and B , μ , η_c , and η_e increase, both $\gamma_{\bar{E}_p}$ and $\eta_{\bar{E}_p}$ decrease.

2. By choosing the appropriate pre-expansion ratio, PM engine cycle can be converted to Otto engine cycle.
3. Under specified conditions of different parameters, thermal efficiencies under the conditions of maximum efficient power and maximum power output are 50.45% and 47.05%, respectively. The latter is about 7.22% higher than the former.
4. Efficient power objective function reflects the compromise between thermal efficiency and power output. The results of this paper can guide parameters selection of the actual heat engine.

Author Contributions: Conceptualization, L.C.; Data curation, Y.G.; Funding acquisition, L.C.; Methodology, P.Z., L.C., and Y.G.; Software, P.Z. and Y.G.; Supervision, L.C.; Validation, P.Z. and Y.G.; Writing—Original draft preparation, P.Z. and L.C.; Writing—Reviewing and Editing, L.C. All authors have read and agreed to the published version of the manuscript.

Funding: This work is supported by the National Natural Science Foundation of China (Project Nos. 52171317 and 51779262) and Graduate Innovative Fund of Wuhan Institute of Technology (Project No. CX2021044).

Institutional Review Board Statement: Not applicable.

Informed Consent Statement: Not applicable.

Data Availability Statement: Not applicable.

Acknowledgments: The authors wish to thank the editor and the reviewers for their careful, unbiased, and constructive suggestions, which led to this revised manuscript.

Conflicts of Interest: The authors declare no conflict of interest.

Nomenclature

B	Heat transfer loss coefficient (W/K)
C_v	Specific heat at constant volume (J/(mol · K))
k	Adiabatic index (-)
\dot{m}	Molar flow rate (mol/s)
P	Power output (W)
Q	Heat transfer rate (W)
R	Gas constant (J/mol/K))
T	Temperature (K)

Greek symbols

γ	Compression ratio (-)
η	Thermal efficiency (-)
η_c	Irreversible compression efficiency (-)
η_e	Irreversible expansion efficiency (-)
μ	Friction loss coefficient (kg/s)
ρ	Pre-expansion ratio(-)
τ	Temperature ratio (-)

Subscripts

in	Input
$leak$	Heat leak
out	Output
max	Maximum value
P	Max power output condition
η	Max thermal efficiency condition
1 – 5	Cycle state points

Superscripts

–	Dimensionless
---	---------------

Abbreviations

- FL Friction loss
- FTT Finite time thermodynamics
- HTL Heat transfer loss
- III Internal irreversibility loss
- OF Objective function
- PM Porous Medium
- SH Specific heats
- WF Working fluid

Appendix A. Performance Indicators with Nonlinear Model of Variable SH

Cycle P is:

$$\begin{aligned}
 P &= \dot{Q}_{in} - \dot{Q}_{out} - P_{\mu} \\
 &= M[2.422 \times 10^{-10}(T_3^3 + T_1^3 - T_2^3 - T_5^3) + 1.6866 \times 10^{-6}(T_3^{2.5} + T_1^{2.5} - T_2^{2.5} - T_5^{2.5}) \\
 &\quad - 6.1567 \times 10^{-6}(T_3^2 + T_1^2 - T_2^2 - T_5^2) + 6.1132 \times 10^{-4}(T_3^{1.5} + T_1^{1.5} - T_2^{1.5} - T_5^{1.5}) + 30.2642 \\
 &\quad (T_3 + T_1 - T_2 - T_5) + 8.7696 \times 10^5(T_3^{-0.5} + T_1^{-0.5} - T_2^{-0.5} - T_5^{-0.5}) + 8.8827 \times 10^6(T_2^{-1} + T_5^{-1} \\
 &\quad - T_1^{-1} - T_3^{-1}) + 3.2074 \times 10^8(T_3^{-2} + T_1^{-2} - T_2^{-2} - T_5^{-2}) + RT_3 \ln \rho] - 64\mu(Ln)^2 \tag{A1}
 \end{aligned}$$

The cycle η is:

$$\begin{aligned}
 \eta &= \frac{P}{\dot{Q}_{in} + Q_{leak}} \\
 &= \frac{M[2.422 \times 10^{-10}(T_3^3 + T_1^3 - T_2^3 - T_5^3) + 1.6866 \times 10^{-6}(T_3^{2.5} + T_1^{2.5} - T_2^{2.5} - T_5^{2.5}) \\
 &\quad - 6.1567 \times 10^{-6}(T_3^2 + T_1^2 - T_2^2 - T_5^2) + 6.1132 \times 10^{-4}(T_3^{1.5} + T_1^{1.5} - T_2^{1.5} - T_5^{1.5}) + 30.2642 \\
 &\quad (T_3 + T_1 - T_2 - T_5) + 8.7696 \times 10^5(T_3^{-0.5} + T_1^{-0.5} - T_2^{-0.5} - T_5^{-0.5}) + 8.8827 \times 10^6(T_2^{-1} + T_5^{-1} \\
 &\quad - T_1^{-1} - T_3^{-1}) + 3.2074 \times 10^8(T_3^{-2} + T_1^{-2} - T_2^{-2} - T_5^{-2}) + RT_3 \ln \rho] - 64\mu(Ln)^2}{\dot{m}[2.422 \times 10^{-10}T^3 + 1.6866 \times 10^{-6}T^{2.5} - 6.1567 \times 10^{-6}T^2 + 6.1132 \times 10^{-4}T^{1.5} + \\
 &\quad 30.2642T + 8.7696 \times 10^5T^{-0.5} - 8.8827 \times 10^6T^{-1} + 3.2074 \times 10^8T^{-2}] \frac{T_3}{T_2} \\
 &\quad + MRT_3 \ln \rho + (B/2)(T_2 + T_3 - 2T_0)} \tag{A2}
 \end{aligned}$$

The cycle E_p is:

$$\begin{aligned}
 E_p &= P\eta \\
 &= \frac{M[2.422 \times 10^{-10}(T_3^3 + T_1^3 - T_2^3 - T_5^3) + 1.6866 \times 10^{-6}(T_3^{2.5} + T_1^{2.5} - T_2^{2.5} - T_5^{2.5}) \\
 &\quad - 6.1567 \times 10^{-6}(T_3^2 + T_1^2 - T_2^2 - T_5^2) + 6.1132 \times 10^{-4}(T_3^{1.5} + T_1^{1.5} - T_2^{1.5} - T_5^{1.5}) + 30.2642 \\
 &\quad (T_3 + T_1 - T_2 - T_5) + 8.7696 \times 10^5(T_3^{-0.5} + T_1^{-0.5} - T_2^{-0.5} - T_5^{-0.5}) + 8.8827 \times 10^6(T_2^{-1} + T_5^{-1} \\
 &\quad - T_1^{-1} - T_3^{-1}) + 3.2074 \times 10^8(T_3^{-2} + T_1^{-2} - T_2^{-2} - T_5^{-2}) + RT_3 \ln \rho] - 64\mu(Ln)^2}{\dot{m}[2.422 \times 10^{-10}T^3 + 1.6866 \times 10^{-6}T^{2.5} - 6.1567 \times 10^{-6}T^2 + 6.1132 \times 10^{-4}T^{1.5} + \\
 &\quad 30.2642T + 8.7696 \times 10^5T^{-0.5} - 8.8827 \times 10^6T^{-1} + 3.2074 \times 10^8T^{-2}] \frac{T_3}{T_2} \\
 &\quad + MRT_3 \ln \rho + (B/2)(T_2 + T_3 - 2T_0)} \tag{A3}
 \end{aligned}$$

Appendix B. Performance Indicators with Model of Constant SH

The expressions of P , η , and E_p of the irreversible PM cycle with constant SH [43] can be obtained as:

$$P = Q_{in} - Q_{out} = M[C_v(T_3 + T_1 - T_2 - T_5) + RT_3 \ln \rho] - 64\mu(Ln)^2 \tag{A4}$$

$$\eta = \frac{P}{Q_{in} + Q_{leak}} = \frac{M[C_v(T_3 + T_1 - T_2 - T_5) + RT_3 \ln \rho] - 64\mu(Ln)^2}{M[C_v(T_3 - T_2) + RT_3 \ln \rho] + B[T_2 + T_3 - 2T_0]} \tag{A5}$$

$$E_p = \frac{[M[C_v(T_3 + T_1 - T_2 - T_5) + RT_3 \ln \rho] - 64\mu(Ln)^2]^2}{M[C_v(T_3 - T_2) + RT_3 \ln \rho] + B[T_2 + T_3 - 2T_0]} \tag{A6}$$

where $C_v = 20.78 J / (mol \cdot K)$ is constant.

Appendix C. Performance Indicators with Linear Model of Variable SH

The SH of the WF is only related to the temperature and has a linear relationship with temperature [44]; the constant SH can be expressed as:

$$C_v = b_v + k_1 T \quad (A7)$$

where b_v and k_1 are constants.

The expressions of P , η , and E_P of the irreversible PM cycle with linear variable SH can be obtained as:

$$P = \dot{Q}_{in} - \dot{Q}_{out} - P_\mu \quad (A8)$$

$$= M[b_v(T_1 + T_3 - T_2 - T_5) + 0.5K(T_1^2 + T_3^2 - T_2^2 - T_5^2) + RT_3 \ln \rho] - 64\mu(Ln)^2_\mu$$

$$\eta = \frac{P}{\dot{Q}_{in} + \dot{Q}_{leak}} \quad (A9)$$

$$= \frac{M[b_v(T_1 + T_3 - T_2 - T_5) + 0.5K(T_1^2 + T_3^2 - T_2^2 - T_5^2) + RT_3 \ln \rho] - 64\mu(Ln)^2}{M[b_v(T_3 - T_2) + 0.5K(T_3^2 - T_2^2) + RT_3 \ln \rho] + MB[T_2 + T_3 - 2T_0]}$$

$$E_P = M[b_v(T_1 + T_3 - T_2 - T_5) + 0.5K(T_1^2 + T_3^2 - T_2^2 - T_5^2) + RT_3 \ln \rho] - 64\mu(Ln)^2 \quad (A10)$$

$$\frac{M[b_v(T_1 + T_3 - T_2 - T_5) + 0.5K(T_1^2 + T_3^2 - T_2^2 - T_5^2) + RT_3 \ln \rho] - 64\mu(Ln)^2}{M[b_v(T_3 - T_2) + 0.5K(T_3^2 - T_2^2) + RT_3 \ln \rho] + MB[T_2 + T_3 - 2T_0]}$$

References

- Andresen, B.; Berry, R.S.; Ondrechen, M.J.; Salamon, P. Thermodynamics for processes in finite time. *Acc. Chem. Res.* **1984**, *17*, 266–271. [[CrossRef](#)]
- Chen, L.G.; Wu, C.; Sun, F.R. Finite time thermodynamic optimization or entropy generation minimization of energy systems. *J. Non-Equilib. Thermodyn.* **1999**, *24*, 327–359.
- Andresen, B. Current trends in finite time thermodynamics. *Angew. Chem. Int. Ed.* **2011**, *50*, 2690–2704.
- Dumitrascu, G.; Feidt, M.; Popescu, A.; Grigorean, S. Endoreversible trigeneration cycle design based on finite physical dimensions thermodynamics. *Energies* **2019**, *12*, 3165.
- Abedinnezhad, S.; Ahmadi, M.H.; Pourkiaei, S.M.; Pourfayaz, F.; Mosavi, A.; Feidt, M.; Shamshirband, S. Thermodynamic assessment and multi-objective optimization of performance of irreversible Dual-Miller cycle. *Energies* **2019**, *12*, 4000. [[CrossRef](#)]
- Feidt, M.; Costea, M.; Feidt, R.; Danel, Q.; Périlhon, C. New criteria to characterize the waste heat recovery. *Energies* **2020**, *13*, 789. [[CrossRef](#)]
- Berry, R.S.; Salamon, P.; Andresen, B. How it all began. *Entropy* **2020**, *22*, 908. [[CrossRef](#)]
- Li, Z.X.; Cao, H.B.; Yang, H.X.; Guo, J.C. Comparative assessment of various low-dissipation combined models for three-terminal heat pump systems. *Entropy* **2021**, *23*, 513. [[CrossRef](#)] [[PubMed](#)]
- Yasunaga, T.; Fontaine, K.; Ikegami, Y. Performance evaluation concept for ocean thermal energy conversion toward standardization and intelligent design. *Energies* **2021**, *14*, 2336. [[CrossRef](#)]
- Sieniutycz, S. *Complexity and Complex Chemo-Electric Systems*; Elsevier: Amsterdam, The Netherlands, 2021.
- Andresen, B.; Salamon, P. Future perspectives of finite-time thermodynamics. *Entropy* **2022**, *24*, 690. [[CrossRef](#)]
- Ge, Y.L.; Chen, L.G.; Sun, F.R. Progress in finite time thermodynamic studies for internal combustion engine cycles. *Entropy* **2016**, *18*, 139. [[CrossRef](#)]
- Ahmadi, M.H.; Pourkiaei, S.M.; Ghazvini, M.; Pourfayaz, F. Thermodynamic assessment and optimization of performance of irreversible Atkinson cycle. *Iran. J. Chem. Chem. Eng.* **2020**, *39*, 267–280.
- Smith, Z.; Pal, P.S.; Deffner, S. Endoreversible Otto engines at maximal power. *J. Non-Equilib. Thermodyn.* **2020**, *45*, 305–310. [[CrossRef](#)]
- Shi, S.S.; Ge, Y.L.; Chen, L.G.; Feng, F.J. Four objective optimization of irreversible Atkinson cycle based on NSGA-II. *Entropy* **2020**, *22*, 1150. [[CrossRef](#)]
- Levario-Medina, S.; Valencia-Ortega, G.; Barranco-Jimenez, M.A. Energetic optimization considering a generalization of the ecological criterion in traditional simple-cycle and combined cycle power plants. *J. Non-Equilib. Thermodyn.* **2020**, *45*, 269–290.
- Ding, Z.M.; Ge, Y.L.; Chen, L.G.; Feng, H.J.; Xia, S.J. Optimal performance regions of Feynman's ratchet engine with different optimization criteria. *J. Non-Equilib. Thermodyn.* **2020**, *45*, 191–207. [[CrossRef](#)]
- Tang, C.Q.; Chen, L.G.; Feng, H.J.; Wang, W.H.; Ge, Y.L. Power optimization of a modified closed binary Brayton cycle with two isothermal heating processes and coupled to variable-temperature reservoirs. *Energies* **2020**, *13*, 3212. [[CrossRef](#)]
- Liu, X.W.; Chen, L.G.; Ge, Y.L.; Feng, H.J.; Wu, F.; Lorenzini, G. Exergy-based ecological optimization of an irreversible quantum Carnot heat pump with spin-1/2 systems. *J. Non-Equilib. Thermodyn.* **2021**, *46*, 61–76. [[CrossRef](#)]

20. Lai, H.Y.; Li, Y.T.; Chan, Y.H. Efficiency enhancement on hybrid power system composed of irreversible solid oxide fuel cell and Stirling engine by finite time thermodynamics. *Energies* **2021**, *14*, 1037. [[CrossRef](#)]
21. Dumitrașcu, G.; Feidt, M.; Grigorean, S. Finite physical dimensions thermodynamics analysis and design of closed irreversible cycles. *Energies* **2021**, *14*, 3416. [[CrossRef](#)]
22. Shi, S.S.; Ge, Y.L.; Chen, L.G.; Feng, F.J. Performance optimizations with single-, bi-, tri- and quadru-objective for irreversible Atkinson cycle with nonlinear variation of working fluid's specific heat. *Energies* **2021**, *14*, 4175. [[CrossRef](#)]
23. Paul, R.; Hoffmann, K.H. A class of reduced-order regenerator models. *Energies* **2021**, *14*, 7295. [[CrossRef](#)]
24. Qiu, S.S.; Ding, Z.M.; Chen, L.G.; Ge, Y.L. Performance optimization of thermionic refrigerators based on van der Waals heterostructures. *Sci. China Technol. Sci.* **2021**, *64*, 1007–1016. [[CrossRef](#)]
25. Badescu, V. Self-driven reverse thermal engines under monotonous and oscillatory optimal operation. *J. Non-Equilib. Thermodyn.* **2021**, *46*, 291–319. [[CrossRef](#)]
26. Qi, C.Z.; Ding, Z.M.; Chen, L.G.; Ge, Y.L.; Feng, H.J. Modelling of irreversible two-stage combined thermal Brownian refrigerators and their optimal performance. *J. Non-Equilib. Thermodyn.* **2021**, *46*, 175–189. [[CrossRef](#)]
27. Valencia-Ortega, G.; Levario-Medina, S.; Barranco-Jiménez, M.A. The role of internal irreversibilities in the performance and stability of power plant models working at maximum e-ecological function. *J. Non-Equilib. Thermodyn.* **2021**, *46*, 413–429. [[CrossRef](#)]
28. Qiu, S.S.; Ding, Z.M.; Chen, L.G.; Ge, Y.L. Performance optimization of three-terminal energy selective electron generators. *Sci. China Technol. Sci.* **2021**, *64*, 1641–1652. [[CrossRef](#)]
29. He, J.H.; Chen, L.G.; Ge, Y.L.; Shi, S.S.; Li, F. Multi-objective optimization of an irreversible single resonance energy-selective electronic heat engine. *Energies* **2022**, *24*, 1074.
30. Chen, Y.R. Maximum profit configurations of commercial engines. *Entropy* **2011**, *13*, 1137–1151. [[CrossRef](#)]
31. Ebrahimi, R. A new design method for maximizing the work output of cycles in reciprocating internal combustion engines. *Energy Convers. Manag.* **2018**, *172*, 164–172. [[CrossRef](#)]
32. Boikov, S.Y.; Andresen, B.; Akhremenkov, A.A.; Tsirlin, A.M. Evaluation of irreversibility and optimal organization of an integrated multi-stream heat exchange system. *J. Non-Equilib. Thermodyn.* **2020**, *45*, 155–171. [[CrossRef](#)]
33. Chen, L.G.; Ma, K.; Feng, H.J.; Ge, Y.L. Optimal configuration of a gas expansion process in a piston-type cylinder with generalized convective heat transfer law. *Energies* **2020**, *13*, 3229. [[CrossRef](#)]
34. Scheunert, M.; Masser, R.; Khodja, A.; Paul, R.; Schwalbe, K.; Fischer, A.; Hoffmann, K.H. Power-optimized sinusoidal piston motion and its performance gain for an Alpha-type Stirling engine with limited regeneration. *Energies* **2020**, *13*, 4564. [[CrossRef](#)]
35. Masser, R.; Hoffmann, K.H. Optimal control for a hydraulic recuperation system using endoreversible thermodynamics. *Appl. Sci.* **2021**, *11*, 5001. [[CrossRef](#)]
36. Paul, R.; Hoffmann, K.H. Cyclic control optimization algorithm for Stirling engines. *Symmetry* **2021**, *13*, 873. [[CrossRef](#)]
37. Khodja, A.; Paul, R.; Fischer, A.; Hoffmann, K.H. Optimized cooling power of a Vuilleumier refrigerator with limited regeneration. *Energies* **2021**, *14*, 8376. [[CrossRef](#)]
38. Badescu, V. Maximum work rate extractable from energy fluxes. *J. Non-Equilib. Thermodyn.* **2022**, *47*, 77–93. [[CrossRef](#)]
39. Paul, R.; Hoffmann, K.H. Optimizing the piston paths of Stirling cycle cryocoolers. *J. Non-Equilib. Thermodyn.* **2022**, *47*, 195–203. [[CrossRef](#)]
40. Li, P.L.; Chen, L.G.; Xia, S.J.; Kong, R.; Ge, Y.L. Total entropy generation rate minimization configuration of a membrane reactor of methanol synthesis via carbon dioxide hydrogenation. *Sci. China Technol. Sci.* **2022**, *65*, 657–678. [[CrossRef](#)]
41. Fischer, A.; Khodja, A.; Paul, R.; Hoffmann, K.H. Heat-only-driven Vuilleumier refrigeration. *Appl. Sci.* **2022**, *12*, 1775. [[CrossRef](#)]
42. Li, J.; Chen, L.G. Optimal configuration of finite source heat engine cycle for maximum output work with complex heat transfer law. *J. Non-Equilib. Thermodyn.* [[CrossRef](#)]
43. Klein, S.A. An explanation for observed compression ratios in international combustion engines. *J. Eng. Gas Turbines Power* **1991**, *113*, 511–513. [[CrossRef](#)]
44. Ghatak, A.; Chakraborty, S. Effect of external irreversibilities and variable thermal properties of working fluid on thermal performance of a Dual internal combustion engine cycle. *J. Mech. Energy* **2007**, *58*, 1–12.
45. Abu-Nada, E.; Al-Hinti, I.; Al-Sarkhi, A.; Akash, B. Thermodynamic modeling of spark-ignition engine: Effect of temperature dependent specific heats. *Int. Commun. Heat Mass Transfer* **2006**, *33*, 1264–1272. [[CrossRef](#)]
46. Angulo-Brown, F.; Rocha-Martinez, J.A.; Navarrete-Gonzalez, T.D. A non-endoreversible Otto cycle model: Improving power output and efficiency. *J. Phys. D Appl. Phys.* **1996**, *29*, 80–83. [[CrossRef](#)]
47. Angulo-Brown, F.; Fernandez, B.J.; Diaz-Pico, C.A. Compression ratio of an optimized Otto-cycle model. *Eur. J. Phys.* **1994**, *15*, 38. [[CrossRef](#)]
48. Chen, L.G.; Zen, F.M.; Sun, F.R. Heat transfer effects on the network output and power as function of efficiency for air standard Diesel cycle. *Energy* **1996**, *21*, 1201–1205. [[CrossRef](#)]
49. Angulo-Brown, F. An ecological optimization criterion for finite-time heat engines. *J. Appl. Phys.* **1991**, *69*, 7465–7469. [[CrossRef](#)]
50. Sahin, B.; Kodal, A.; Yavuz, H. Efficiency of a Joule-Brayton engine at maximum power density. *J. Phys. D Appl. Phys.* **1995**, *28*, 1309. [[CrossRef](#)]
51. Yan, Z.J. η and P of a Carnot engine at maximum ηP . *Chin. J. Nat.* **1984**, *7*, 475. (In Chinese)

52. Gonca, G.; Genc, I. Thermoecology-based performance simulation of a Gas-Mercury-Steam power generation system (GMSPGS). *Energy Convers. Manag.* **2019**, *189*, 91–104. [[CrossRef](#)]
53. Gonca, G.; Genc, I. Performance simulation of a double-reheat Rankine cycle mercury turbine system based on exergy. *Int. J. Exergy* **2019**, *30*, 392–403. [[CrossRef](#)]
54. Chen, L.G.; Tang, C.Q.; Feng, H.J.; Ge, Y.L. Power, efficiency, power density and ecological function optimizations for an irreversible modified closed variable-temperature reservoir regenerative Brayton cycle with one isothermal heating process. *Energies* **2020**, *13*, 5133. [[CrossRef](#)]
55. Diskin, D.; Tartakovsky, L. Efficiency at maximum power of the low-dissipation hybrid electrochemical–otto cycle. *Energies* **2020**, *13*, 3961. [[CrossRef](#)]
56. Wang, R.B.; Chen, L.G.; Ge, Y.L.; Feng, H.J. Optimizing power and thermal efficiency of an irreversible variable-temperature heat reservoir Lenoir cycle. *Appl. Sci.* **2021**, *11*, 7171. [[CrossRef](#)]
57. Gonca, G.; Hocaoglu M, F. Exergy-based performance analysis and evaluation of a dual-diesel cycle engine. *Therm. Sci.* **2021**, *25*, 3675–3685. [[CrossRef](#)]
58. Gonca, G.; Sahin, B. Performance investigation and evaluation of an engine operating on a modified dual cycle. *Int. J. Energy Res.* **2022**, *46*, 2454–2466. [[CrossRef](#)]
59. Paul, R.; Khodja, A.; Fischer, A.; Masser, R.; Hoffmann, K.H. Power-optimal control of a Stirling engine’s frictional piston motion. *Entropy* **2022**, *24*, 362. [[CrossRef](#)]
60. Bellos, E.; Lykas, P.; Tzivanidis, C. Investigation of a solar-driven organic Rankine cycle with reheating. *Appl. Sci.* **2022**, *12*, 2322. [[CrossRef](#)]
61. Yilmaz, T. A new performance criterion for heat engines: Efficient power. *J. Energy Inst.* **2006**, *79*, 38–41. [[CrossRef](#)]
62. Atmaca, M.; Gümüř, M.; Demir, A. Comparative thermodynamic analysis of dual cycle under alternative conditions. *Therm. Sci.* **2011**, *15*, 953–960. [[CrossRef](#)]
63. Reyes-Ramírez, I.; Barranco-Jiménez, M.A.; Rojas-Pacheco, A.; Guzmán-Vargas, L. Global stability analysis of a Curzon–Ahlborn heat engine under different regimes of performance. *Entropy* **2014**, *16*, 5796–5809. [[CrossRef](#)]
64. Kumar, R.; Kaushik, S.C.; Kumar, R. Performance optimization of Brayton heat engine at maximum efficient power using temperature dependent specific heat of working fluid. *J. Therm. Eng.* **2015**, *1*, 345–354. [[CrossRef](#)]
65. Gonca, G. Performance analysis of an Atkinson cycle engine under effective power and effective power density condition. *Acta Phys. Polon.* **2017**, *132*, 1306–1313. [[CrossRef](#)]
66. Gonca, G.; Hocaoglu, M.F. Performance Analysis and Simulation of a Diesel-Miller Cycle (DiMC) Engine. *Arabian J. Sci. Eng.* **2019**, *44*, 5811–5824. [[CrossRef](#)]
67. Gonca, G.; Sahin, B. Performance analysis of a novel eco-friendly internal combustion engine cycle. *Int. J. Energy Res.* **2019**, *43*, 5897–5911. [[CrossRef](#)]
68. Gonca, G.; Sahin, B.; Genc, I. Investigation of maximum performance characteristics of seven-process cycle engine. *Int. J. Exergy* **2022**, *37*, 302–312. [[CrossRef](#)]
69. Nilavarasi, K.; Ponnuragan, M. Optimized efficiency at maximum figure of merit and efficient power of power law dissipative Carnot like heat engines. *J. Stat. Mech. Theory Exp.* **2021**, *4*, 043208. [[CrossRef](#)]
70. Ferrenberg, A.J. The Single Cylinder Regenerated Internal Combustion Engine. In Proceedings of the Earthmoving Industry Conference & Exposition, Canoga Park, CA, USA, 1 April 1990. [[CrossRef](#)]
71. Howell, J.R.; Hall, M.J.; Ellzey, J.L. Combustion of hydrocarbon fuels within porous inert media. *Prog. Energy Combust. Sci.* **1996**, *22*, 121–145. [[CrossRef](#)]
72. Durst, F.; Weclas, M. A new type of internal combustion engine based on the porous-medium combustion technique. *Proc. Inst. Mech. Eng. D J. Automob. Eng.* **2001**, *215*, 63–81. [[CrossRef](#)]
73. Liu, H.S.; Xie, M.Z.; Chen, S. Thermodynamic analysis of ideal cycle of porous media (PM). *J. Eng.* **2006**, *27*, 553–555. (In Chinese)
74. Liu, H.S.; Xie, M.Z.; Wu, D. Thermodynamic analysis of the heat regenerative cycle in porous medium engine. *Energy Convers. Manag.* **2009**, *50*, 297–303. [[CrossRef](#)]
75. Ge, Y.L.; Chen, L.G.; Sun, F.R. Thermodynamic modeling and parametric study for porous medium engine cycles. *Termotehnika* **2009**, *13*, 49–55.
76. Zang, P.C.; Ge, Y.L.; Chen, L.G.; Gong, Q.R. Power density characteristic analysis and multi-objective optimization of an irreversible porous medium engine cycle. *Case Stud. Therm. Eng.* **2022**, *35*, 102154. [[CrossRef](#)]
77. Zang, P.C.; Chen, L.G.; Ge, Y.L.; Shi, S.S. Four-objective optimization for an irreversible porous medium cycle with linear variation in working fluid’s specific heat. *Entropy* **2022**, *24*, 1074. [[CrossRef](#)] [[PubMed](#)]